Electron spin resonance of Fe^{3+} centres in alpha -TeO_2:Fe

1995 J. Phys.: Condens. Matter 7 2889

(http://iopscience.iop.org/0953-8984/7/14/025)

J. Phys.: Condens. Matter 7 (1995) 2889–2899. Printed in the UK

Electron spin resonance of Fe^{3+} centres in α-TeO_2:Fe

K Raksányi†, A Watterich†, O R Gilliam‡, L A Kappers‡ and G J Edwards‡§

† Research Laboratory for Crystal Physics, Hungarian Academy of Sciences, Budaörsi út 45, H-1112 Budapest, Hungary

‡ Department of Physics and Institute of Materials Science, University of Connecticut, Storrs, CT 06269-3136, USA

Received 30 August 1994, in final form 12 December 1994

Abstract. Two prominent Fe^{3+} centres were observed by ESR in α-TeO_2:Fe single crystals. One of them exhibits C_2 symmetry ($Fe^{3+}(C_2)$ centre) and the other one exhibits C_1 symmetry and also superhyperfine interactions with two hydrogens (Fe^{3+}–2H–$V_o(C_1)$ centre). The $Fe^{3+}(C_2)$ centre is believed to be an interstitial Fe^{3+} ion; the nature of its superhyperfine interaction with neighbouring Te nuclei contributes to this assignment. The Fe^{3+}–2H–$V_o(C_1)$ centre is attributed to a substitutional Fe^{3+} ion with two neighbouring hydrogens and a local oxygen vacancy.

1. Introduction

Paratellurite (α-TeO_2) is a transparent crystal with excellent acousto-optic features used in modulators, deflectors, tunable filters and other optical devices. Foreign ions are of great significance either as unwanted impurities, which impair crystal quality, or as possible modifiers of the basic crystal properties.

Földvári *et al* [1] found that the most prominent impurities in paratellurite are Pt (from the crucible) and Fe (from the raw material); they reported the joint incorporation of these impurities. Malicskó and Krajewski [2] showed, by scanning electron microscopy, enhanced concentrations of impurities in the defects visible by optical microscopy, e.g. aggregates and bubbles. However, via the use of extra-pure raw materials the production of gas bubbles could be avoided [3]. In Fe-doped TeO_2 the optical absorption spectrum was reported [4] and it was concluded that the Fe aggregates and easily forms precipitates if one attempts to dope the crystals to concentrations higher than 0.03 mol%.

We have previously conducted electron spin resonance (ESR) studies on TeO_2 crystals containing Pt [5], V [6] and Cr [7] impurity or dopants. It was shown that Pt^{3+} enters the lattice substitutionally without any nearby disturbance, preserving the original C_2 symmetry of a Te site. The V^{4+} ion enters the crystal substitutionally as well, although its environment possesses two symmetrically located hydrogens, whose presence was verified by ENDOR. In TeO_2:Cr three Cr^{3+} centres were observed, two of them in as-grown crystals. One type of Cr^{3+} centre was the plain substitutional Cr^{3+} ion with C_2 symmetry. The second Cr^{3+} centre exhibited superhyperfine (SHF) interaction with two neighbouring hydrogen ions and its symmetry was C_1. To explain the lower C_1 symmetry a nearby oxygen vacancy was included in the defect model. The centre was denoted, therefore, as Cr^{3+}–2H–V_o, where V_o is the notation for an oxygen vacancy. The hydrogen ions in this centre could be removed by a low-temperature electron irradiation and detected as trapped H^0 atoms. The Cr^{3+} centre

§ Present address: Department of Physics, West Virginia University, Morgantown, WV 26506, USA.

0953-8984/95/142889+11$19.50

remaining after the electron irradiation could also be generated by annealing the sample at 620 °C in an oxygen atmosphere. It was designated as a Cr^{3+}–V_o centre because of its C_1 symmetry and the lack of any SHF interaction.

In this paper we report the ESR study of Fe-doped TeO_2. Two prominent Fe^{3+} centres were detected. The ESR characterization of these centres will be given; also the computer fitting method will be described. Since the tetragonal crystal structure of paratellurite may be regarded as a distorted rutile structure with doubling of the unit cell along the c axis [8], comparison will be made with Fe^{3+} centres reported for rutile-type crystals [9–12].

2. Experiment details and fitting methods

2.1. Experimental details

Single crystals of paratellurite were grown by a balance-controlled Czochralski technique [13] using a platinum crucible and resistance heating. The TeO_2 starting material was prepared from pure (< 5 ppm) Te metal to which 0.03 mol% Fe_2O_3 was added. The samples were x-ray oriented and cut to typical sizes of $9 \times 3 \times 2$ mm^3. In order to avoid Fe aggregates and precipitates, we used the colourless parts of the boules. ESR measurements were performed at temperatures of 92 and 10 K using an X band spectrometer.

2.2. Fitting the spin Hamiltonian parameters

A brief description of our computer program for fitting the spin Hamiltonian parameters was given in an earlier paper [7]. Since then it has been significantly improved to handle problems of higher spin number. Our model spin Hamiltonian, restricted to second-order Zeeman terms, can be written for $S = \frac{5}{2}$ and for C_2 symmetry by reference to [14]

$$\mathcal{H}_s = \beta(B_x g_{xx} S_x + B_y g_{yy} S_y + B_z g_{zz} S_z) + B_2^0 O_2^0 + B_2^2 O_2^2 + B_4^0 O_4^0 + B_4^2 O_4^2 + B_4^4 O_4^4 + C_2^2 \Omega_2^2 + C_4^2 \Omega_4^4 + C_4^4 \Omega_4^4. \quad (1)$$

For C_1 symmetry the following terms should be added:

$$B_2^1 O_2^1 + B_4^1 O_4^1 + B_4^3 O_4^3 + C_2^1 \Omega_2^1 + C_4^1 \Omega_4^1 + C_4^3 \Omega_4^3. \quad (2)$$

For comparison with earlier ESR results on high-spin Fe^{3+} ions the following equalities exist:

$$D = 3B_2^0 \qquad E = B_2^2 \qquad F = 180B_4^0 - 36B_4^4 \qquad a = 24B_4^4.$$

These equations hold only if the eigenvectors of the corresponding second- and fourth-order equivalent zero-field splitting (ZFS) spin operators are equal and these operator components are rotated into the common eigenvector system. However, if the values of the other coefficients pertaining to the tensor operators are small, the fitted values in the present work can be compared with the parameters obtained in experiments with higher symmetry and converted by the above equations.

Following [14] the coordinate system of our model spin Hamiltonian is equal to the eigenvector system of the **g** matrix. Three Euler angles for C_1 or one for C_2 symmetry are included into the list of the adjustable parameters. The appearance of non-zero values of the parameters B_2^1, C_2^1 and C_2^2 reflect the misfit between the eigenvector systems of **g** and

the second-order ZFS matrix. The number of fourth-order ZFS-type spin tensor operators is generally nine for C_1 symmetry, and three of them also specify the corresponding misfit. The eigenvector systems of the second- and fourth-order ZFS-type spin tensor operators are determined by Euler rotations, which reduce the number of operator components to two or six, respectively. These eigenvector systems may turn out to be different.

The case of fourth-order Zeeman terms is more problematic. As was pointed out by Grachev [15], the appearance of redundant parameters can be expected to an increasing degree for lower symmetries. Although not stated explicitly, the redundance is somehow linked with irreps (irreducible representations) of odd order. For C_1 symmetry the number of possible fourth-order parameters is $3*7 = 9+7+5 = 21$. Omitting the odd third-order irrep reduces the number to 14. For C_2 symmetry, terms having odd subspecie indices in the $B*S*S*S$ coupling should be omitted, resulting eventually in non-redundant parameter sets of 14 (C_1) and eight (C_2).

Our program has built-in capabilities to handle the six fourth-order Zeeman terms given by Altschuler and Kosyrev [14] for C_{2v} symmetry:

$$g_4^1 O_3^1,\ g_4^3 O_3^3,\ \Gamma_4^1 \Omega_3^1,\ \Gamma_4^2 \Omega_3^2,\ g_4^0 O_3^0 \text{ and } g_4^2 O_3^2.$$

These parameters are probably non-redundant in C_2 symmetry. They were varied individually and independently for both symmetries, keeping the ZFS and the second-order Zeeman parameters constant at their optimized values. The fitting procedure brought about either an insignificant gain in the value of the least-squares fitting function, or the parameters were pushed towards negligible values. This result indicates the insignificance of fourth-order Zeeman parameters for the centres investigated. The number of adjustable parameters amounts to 3 + (6) Zeeman+8 ZFS+1 Euler angle coefficient for C_2 symmetry and 3 + (6) Zeeman+14 ZFS+3 Euler angle coefficients for C_1 symmetry, where parentheses point to parameters that were found to be negligibly small. In addition, for both symmetries the tilt angles to allow for minor crystal misorientation for each plane are also included in the list of the adjustable parameters.

The orientations of magnetic field vectors are given with respect to rotations around the normals of given numbers of crystal orientation planes. The rotation angles can be varied by equidistant increments or specified as an arbitrary set. The frequency of the oscillating magnetic field is kept constant within a sample rotation cycle, but can be varied with respect to different crystal planes. The different orientations of the same type of centres with respect to the magnetic field (families) are produced by the crystal symmetry transformation matrices.

In the simulation mode, the program sets up the spin Hamiltonian using probe magnetic field values as input and scans the magnetic field until obtaining transition frequencies adjusted exactly to the experimental frequency. The magnetic field values are listed for all adjustable transitions and, after checking the transition moments, a selection of transitions is carried out for later calculations using the fitting mode. This mode could also be used for direct fitting, but the additional scanning cycle makes the procedure more time consuming. In the fitting mode, therefore, the frequencies of the previously selected transitions are calculated by applying experimental field values in the spin Hamiltonian. The square sum of the differences between experimental and calculated frequencies weighted by factors calculated from the derivatives of the frequencies with respect to the adjustable parameters is minimized by the conjugate gradient method of Murtagh and Sargent [16].

3. Experimental results and discussion

After doping TeO_2 crystals with iron, it is logical to assume that new ESR spectra will be due to iron ions. Typical chemical states for the iron dopant would be Fe^{2+}, Fe^{3+} and Fe^{4+} ions. Of these, however, only the Fe^{3+} ion, which has an unfilled shell with an *odd* number of electrons, is easily observed by ESR, since its spin degeneracy is not removed until application of the external magnetic field. In prior spin resonance studies of rutile-type crystals, iron dopant has been reported as $Fe^{3+}(3d^5)$ ions in the high-spin state with $S = \frac{5}{2}$ [9–12]. For this S value, ESR transitions may occur between six spin states. Normally no hyperfine interaction is detectable for Fe^{3+} ions since the only naturally occurring isotope of Fe with nuclear spin has low abundance and a very small nuclear magnetic moment (^{57}Fe, $I = \frac{1}{2}$, 2.19% abundance, $0.09\mu_N$ [17]).

Four different Te sites exist in the unit cell of TeO_2. Thus for a substitutional cation one expects four different orientations with respect to the magnetic field. If this cation exhibits spin resonance, the four inequivalent sites yield four families of spectra for the same electron spin transition. If the centre is disturbed by a nearby defect, the symmetry typically is reduced from C_2 to C_1 and the number of families is increased to eight.

From symmetry considerations and angular variation studies of the ESR spectra, two centres attributable to Fe^{3+} ions have been distinguished. One exhibits C_2 symmetry and will be designated as the $Fe^{3+}(C_2)$ centre; the other exhibits C_1 symmetry and will be denoted as the Fe^{3+}–2H–$V_o(C_1)$ centre (similar notation to that used earlier for a Cr^{3+} centre). Both centres have been fitted to the spin Hamiltonian given by (1) and (2) with $S = \frac{5}{2}$. Their respective energy levels are shown in figure 1(*a*) and (*b*) for $\boldsymbol{B} \parallel [001]$; these were calculated from optimized spin Hamiltonian parameters. For any selected magnetic field value the levels will be numbered in order of increasing energy from 1 to 6. All possible transitions for a microwave frequency of 9.1 GHz are indicated in the figure. For $Fe^{3+}(C_2)$ one spin transition was found between energy levels 1 and 2 and energy levels 3 and 4, and two transitions between the energy levels 2 and 3 (figure 1(*a*)). For Fe^{3+}–2H–$V_o(C_1)$ centres transitions between the energy levels 1 and 2 and 3 and 4 were observed (figure 1(*b*)). The observed transitions are specifically noted by arrows on these energy level diagrams.

Figure 2 shows an ESR spectrum of the $Fe^{3+}(C_2)$ centre consisting of a family of four main lines; this signifies four inequivalent sites and symmetry C_2. The figure also shows satellite lines for each family, which are attributed to two pairs of ^{125}Te superhyperfine (SHF) lines. The spectrum represents the 3–4 transition and was taken at 10 K, 9.1 GHz and an orientation approximately 2° away from $\boldsymbol{B} \parallel [100]$. Most of the Te isotopes have nuclear spin $I = 0$ and these isotopes have a net natural abundance of 91.98%. Tellurium has two isotopes with $I = \frac{1}{2}$; these are ^{125}Te (7.12% abundant) and ^{123}Te (0.90% abundant) [17]. Their magnetic moments differ by a factor of 1.2 with $^{125}\mu > {}^{123}\mu$ but the ^{125}Te SHF lines have intensities eight times those of the ^{123}Te isotope and are dominant in the SHF spectra. From the isotopic abundances the expected intensity ratio of the main line to the SHF lines from a single ^{125}Te site would be 26:1. The average observed ratios of a main line and SHF lines labelled 1 and 2 in figure 2 are approximately 26:2.2 and 26:4.4, respectively. These ratios can be explained by assuming SHF interaction with a single ^{125}Te nucleus in one of two and four magnetically equivalent Te sites, respectively, where the influence of the ^{123}Te isotope has been neglected.

The eight families of the Fe^{3+}–2H–$V_o(C_1)$ centres are shown in figure 3 for an ESR observation made at 92 K, 9.1 GHz and approximately 5° from $\boldsymbol{B} \parallel [001]$. They correspond to the 3–4 energy transition for this centre. (The four lines of the $Fe^{3+}(C_2)$ centre at

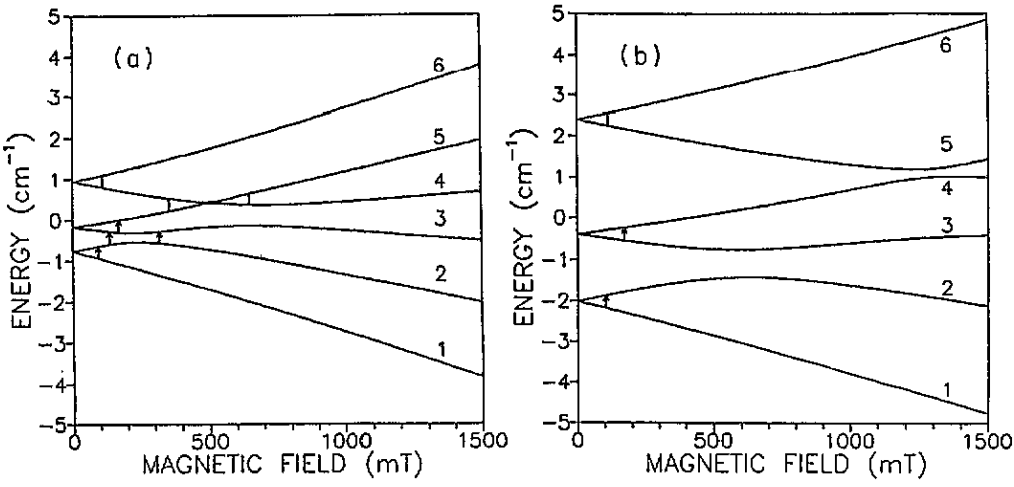

Figure 1. The energy levels for Fe centres in TeO_2 as a function of external magnetic field for $B \parallel [001]$. Transitions observed at 9.1 GHz are indicated by arrows. The energy levels were calculated with optimized spin Hamiltonian parameters. On the figure they are shown numbered in order of increasing energy for high magnetic fields; at low fields for figure (*a*) the numbers for levels 4 and 5 are reversed. (*a*) $Fe^{3+}(C_2)$ centre; (*b*) Fe^{3+}–2H–$V_O(C_1)$ centre.

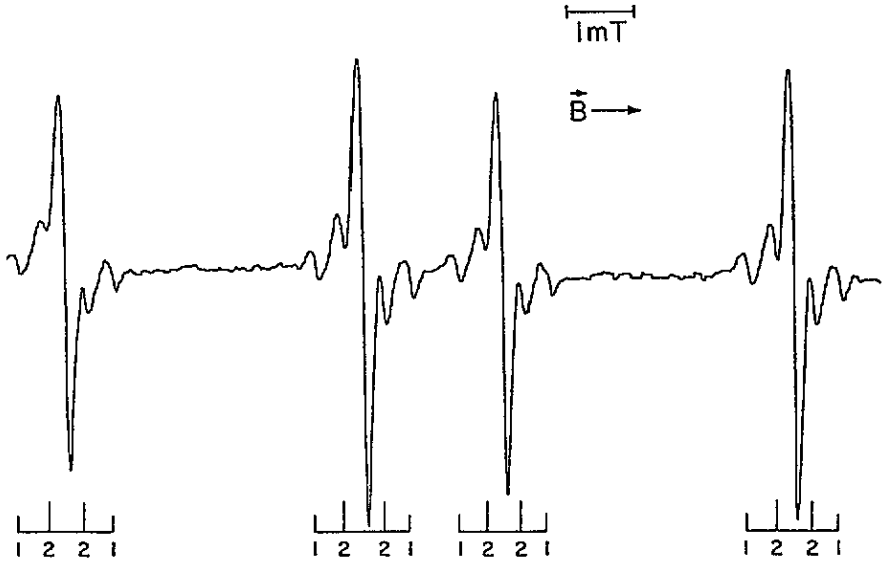

Figure 2. ESR spectrum of the $Fe^{3+}(C_2)$ centre (for spin transitions between energy levels 3 and 4) in a single crystal of TeO_2:Fe whose orientation was approximately 2° away from $B \parallel [100]$. Each of the four groups (due to four inequivalent sites) exhibits ^{125}Te SHF splittings. The spectrum was taken at 10 K and ~ 9.1 GHz.

lower fields represent its lower-field 2–3 energy transition and the two lines at higher field represent the 3–4 transition.) Each of the eight Fe^{3+}–2H–V_O main lines is split into three lines or triplets with approximately 1:2:1 intensity ratios, where this value of the ratio is most

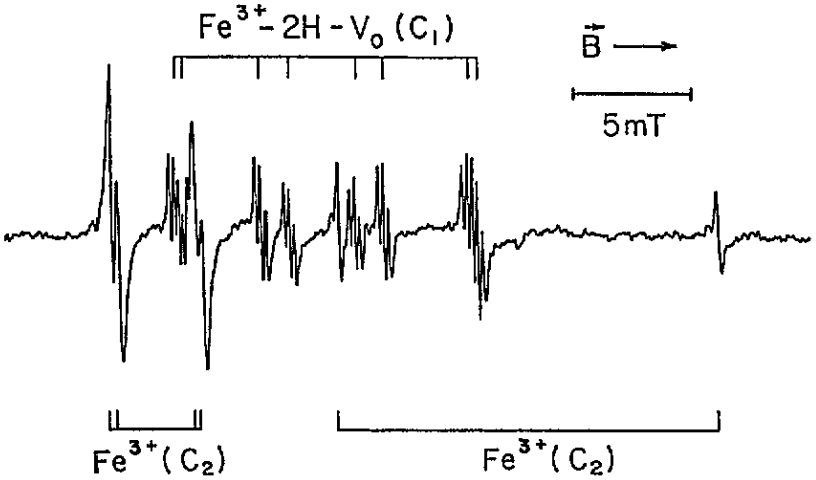

Figure 3. The ESR spectrum of the Fe^{3+}–2H–$V_o(C_1)$ centre in TeO_2:Fe corresponding to the 3–4 energy transition. There are eight line groups, each group consisting of a triplet with intensity ratios approximately 1:2:1. The triplets are due to SHF interactions with two nearly equivalent protons. The spectrum also shows the $Fe^{3+}(C_2)$ centre, where the four lines at lower fields correspond to the lower-field transitions between energy levels 2 and 3, and the two lines at higher fields correspond to transitions between energy levels 3 and 4. The observation was made at 92 K, ~ 9.1 GHz and 5° from $B\|$ [001].

readily seen in the middle four of the eight triplets. These splittings are like those observed for V^{4+} [6] and Cr^{3+} [7] ions in TeO_2, which were attributed to SHF interactions with two neighbouring hydrogen impurity ions. The approximate 1:2:1 intensity ratio results from two nearly magnetically equivalent, $I = \frac{1}{2}$, 100% abundant isotopes. Although a complete angular variation study of this SHF interaction was not feasible, the magnitude of the splitting is quite similar to that observed for V and Cr ions. Since the crystal was grown in air, it is expected that hydrogen enters the lattice in the form of OH^- ions. We conclude that two nearly equivalent hydrogens ($I = \frac{1}{2}$, natural abundance 100%) cause the SHF splittings and the nearly 1:2:1 intensity ratios.

It should be mentioned that besides Fe^{3+}, V^{4+} [6] and Cr^{3+} [7], we have also observed that Mn^{4+} and Co^{2+} show similar hydrogen SHF structure in TeO_2. The latter two paramagnetic ions have not been studied in detail. Although the observed hydrogen SHF interaction suggests the presence of two OH^- ions near the V^{4+} or Mn^{4+} ion, it is clear that the role of the OH^- ions is not charge compensation as it is, for example, in the TiO_2:Fe crystal [18]. The oxygen octahedron is much more distorted in the more covalent paratellurite than in the more ionic rutile crystal. Cation substitution of transition metal dopants is more difficult in the distorted lattice, as indicated by strong inclination towards aggregation and precipitation of these ions in paratellurite. However, the presence of two OH^- ions is presumed to make the Te site a more accommodating position for impurity ions. The O–O distances in TeO_2 are close to the usual OH···O distances. The fact that we could not observe an infrared (IR) absorption band due to these OH-related centres may stem from the presence of very broad IR bands; in fact strong hydrogen bridging is known to broaden the IR bands [19]. We have seen that despite two nearby hydrogens, the substitutional V^{4+} ion preserves the original C_2 symmetry of the Te site [6]. Yet, analogous to one of the Cr^{3+} centres in TeO_2 [7], an additional defect such as an oxygen vacancy is believed to perturb

the Fe^{3+}–2H complex leading to the reduced C_1 symmetry. Thus the centre is denoted as Fe^{3+}–2H–$V_o(C_1)$.

To facilitate a determination of the spin Hamiltonian parameters, angular variation studies were made. For the two $Fe^{3+}(3d^5)$ defects denoted as $Fe^{3+}(C_2)$ and Fe^{3+}–2H–$V_o(C_1)$, angular variations were made in two different planes. One plane for each centre is shown in figure 4. The solid lines in figure 4 are computer-simulated angular variations calculated every 5° with the optimized spin Hamiltonian parameters, obtained using $S = \frac{5}{2}$ and (1) and (2). The non-zero ZFS spin Hamiltonian parameters are presented in table 1, where they are compared with Fe^{3+} centres reported for various rutile-like hosts. In table 2 the principal values and eigenvectors of the **g** matrices for the Fe^{3+} centres are given and compared with those of Cr^{3+} centres in TeO_2. The principal axes were assigned using the convention of minimizing the ratio $|B_2^2/3B_2^0|$, which is approximately equivalent to the ratio $|E/D|$ in another common spin Hamiltonian notation.

We have seen in [7] that the D (or $3B_2^0$) value does not differ much for the plain Cr^{3+} centres in different rutile-type hosts. For a plain substitutional Fe^{3+} centre we could estimate a D value similar to the values given for Fe^{3+} in table 1 for other rutile-type crystals. For the Fe^{3+}–2H–V_o centre, since the determined D value does not differ too much from the average D value of the plain Fe^{3+} in other rutile-type hosts, we suggest that the perturbing oxygen vacancy V_o is not the nearest neighbour of the Fe ion in the Fe^{3+}–2H–V_o centre. A nearest-neighbour vacancy would be expected to provide a very different crystalline electric field for the centre, perhaps similar to that reported for the oxygen vacancy associated with Fe^{3+} in $SrTiO_3$ [20], or the one calculated with the superposition model for Cr^{3+}–V_{oI} in SnO_2 [21]. Although the Fe^{3+}–2H–V_o centre is closely related to the Cr^{3+}–2H–V_o centre, the difference of their eigenvectors (table 2) indicates different V_o positions.

The D value of the $Fe^{3+}(C_2)$ centre differs strongly from the average D value of the plain Fe^{3+} centres in other rutile-type hosts (table 1). This is one of the reasons we do not attribute this centre to the plain Fe^{3+} centre. Furthermore, the Te SHF pattern differs markedly from those for substitutional ions in TeO_2; for substitutional Cr^{5+} we have seen three different Te SHF interactions, where the two stronger ones were each due to interactions with Te nuclei in two separate but magnetically equivalent sites, while the weakest one was with Te nuclei in one unique site [22]. With allowance for the C_2 symmetry of the $Fe^{3+}(C_2)$ centre, the following models can be proposed for this centre:

(i) an Fe^{3+} ion at a cation site associated with two nearest-neighbour symmetrically arranged oxygen vacancies and

(ii) an Fe^{3+} ion in an interstitial position between two Te atoms in the [001] direction, or shifted from this position along the C_2 symmetry axis.

The first model should be ruled out since it does not yield the correct intensity ratios for the Te SHF lines. However, the second model is consistent with the SHF relative intensities of 2:4:4:2. This interstitial model is shown in figure 5. Two approximately equivalent Te atoms (numbers 5 and 10) are nearest neighbours to the interstitial Fe ion and yield the larger SHF splitting, and four nearly equivalent Te atoms (numbers 6–9) contribute to overlapping SHF splittings with half as much splitting and twice the intensity as that due to Te atoms 5 and 10.

4. Conclusions

Two prominent Fe^{3+} centres were observed by ESR in TeO_2:Fe single crystals. One of them possesses C_2 symmetry ($Fe^{3+}(C_2)$ centre) and the other one C_1 symmetry (Fe^{3+}–2H–$V_o(C_1)$

Table 1. Non-zero ZFS parameters of Fe^{3+} centres in different rutile-type crystals given in units of cm^{-1}. In TeO_2 the measurements were made at ~ 9.1 GHz and 92 K. Fe_i^{3+} denotes an interstitial iron ion; V_{oI} stands for an oxygen vacancy in the first sphere around the Fe dopant ion.

Host	Centre	$D = 3B_2^0$	$E = B_2^2$	B_4^0	B_4^4		Reference
	Fe^{3+}	0.678	0.074	−0.0001	0.0015		[9]
TiO_2	Fe^{3+}–V_{oI}	0.763	0.090	0.0018	−0.0001		[10]
	Fe_i^{3+}–H	0.437	0.077	0.0011	0.0005		[10]
SnO_2	Fe^{3+}	0.8651	0.0899	−0.0001	0.0001		[11]
	Fe^{3+}–H	1.2876	−0.0477	−0.01	−0.001		[12]
		D	E	B_4^0	B_4^2		
	$Fe^{3+}(C_2)$	0.284 ± 0.003	0.033 ± 0.001	$(-15 \pm 5) \times 10^{-6}$	$(-19 \pm 4) \times 10^{-5}$		
TeO_2	Fe^{3+}–2H–$V_o(C_1)$	0.717 ± 0.003	0.087 ± 0.001	—	$(14 \pm 5) \times 10^{-5}$		This work
		C_2^2	C_4^2	B_4^1	C_2^1	C_4^1	
		$(6 \pm 1) \times 10^{-4}$	$(8 \pm 2) \times 10^{-5}$	$(-44 \pm 2) \times 10^{-5}$	$(-30 \pm 5) \times 10^{-4}$	$(25 \pm 2) \times 10^{-5}$	

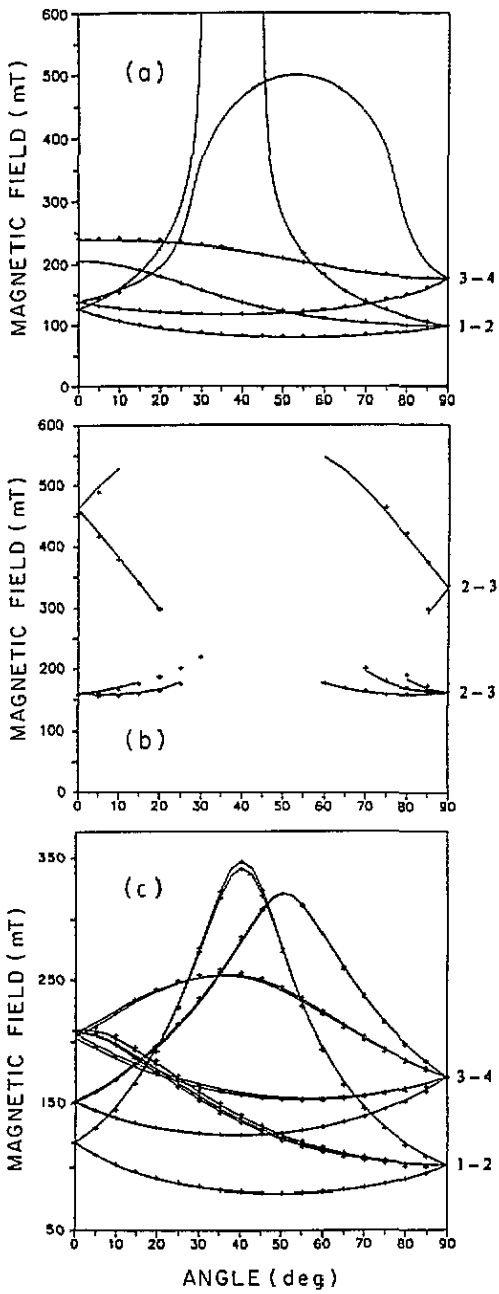

Figure 4. Angular variations of ESR line positions for two different Fe^{3+} centres in Fe-doped TeO_2. The crosses represent experimental data and the solid curves are computer-simulated angular variations using optimized spin Hamiltonian parameters and sample tilt angles. Measurements were made at 92 K and ~ 9.1 GHz. The energy level transitions are indicated. (*a*, *b*) For the $Fe^{3+}(C_2)$ centre, where the angles 0° and 90° correspond to ***B*** along [110] and [001] directions, respectively. (*c*) For the Fe^{3}–2H–$V_o(C_1)$ centre, where the angles 0° and 90° correspond only approximately to ***B*** along [110] and [001] directions, respectively; therefore all possible transitions due to the different families or groups are observed.

Table 2. Principal values and eigenvectors of the **g** matrices for Fe^{3+} centres compared with those of Cr^{3+} centres in TeO_2, where the direction cosines of the dimensionless eigenvectors x, y and z are defined with respect to the crystallographic axes [100], [010] and [001]. The axes were assigned according to the convention of minimizing the ratio $|E/D|$. Estimated errors for the direction cosines are ±0.003.

Centre (in α-TeO_2)	g_{xx}	g_{yy}	g_{zz}	x	y	z	Reference
				0.707	0.696	−0.127	
Cr^{3+}	1.980	1.983	1.976	−0.707	0.696	−0.127	
				0.000	0.180	0.984	
							[7]
	1.998	1.990	1.992	0.497	0.864	−0.076	
Cr^{3+}–2H–V_o				−0.823	0.441	−0.358	
				0.276	0.241	0.931	
				0.707	0.426	−0.564	
$Fe^{3+}(C_2)$	2.004	1.989	1.999	−0.707	0.426	−0.564	
				0.000	0.798	0.602	
							This work
				0.463	0.433	−0.774	
Fe^{3+}–2H–$V_o(C_1)$	2.002	1.999	1.998	−0.845	0.479	−0.237	
				0.268	0.764	0.587	

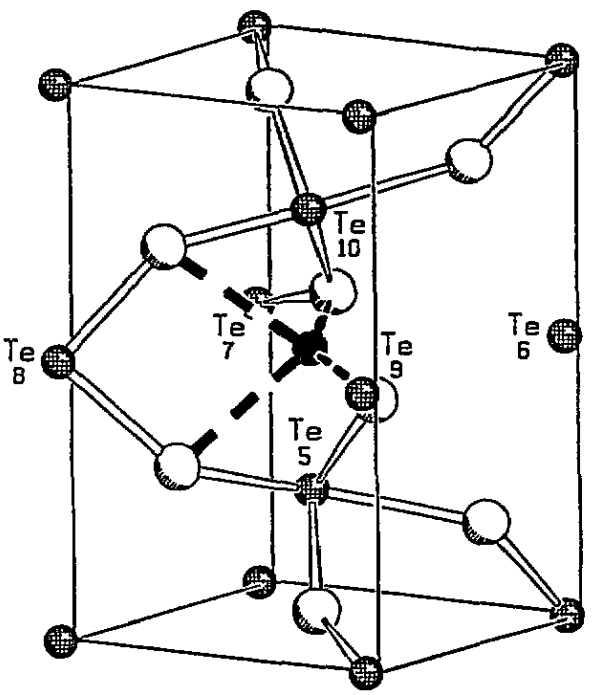

Figure 5. A model for interstitial Fe in TeO_2. The Fe ion is indicated with black, the Te ion is shaded and the O ions are open circles. The possible bonds of the Fe ion to the nearest O ions are marked with dashed bonds. The model was created by a computer program called SCHAKAL 92/V256 (E Keller, Crystallographic Institute, University of Freiburg, Freiburg, Germany).

centre) while showing also two hydrogen SHF interactions. Based on the strong contrast of the D value of the $Fe^{3+}(C_2)$ centre with the D values reported for other rutile-type hosts, and based on the characteristics of the observed Te SHF interactions, this centre is attributed to an interstitial Fe^{3+} ion. The Fe^{3+}–2H–V_o centre is assigned to a substitutional Fe^{3+} cation with two neighbouring hydrogens and an oxygen vacancy as a near but not nearest neighbour to the Fe^{3+} ion. The presence and nearly symmetrical arrangement of two hydrogens about the cation dopant seem typical for doped TeO_2, since besides Fe^{3+}, they were also observed around V^{4+}, Cr^{3+}, Co^{2+} and Mn^{4+} ions. The hydrogens are considered part of two hydroxyl ions, which produce more accommodating surroundings for the foreign ion in the rather covalent, and therefore strongly distorted, paratellurite lattice.

Acknowledgments

This research was supported by the US National Science Foundation under grant No INT-9222297, the University of Connecticut Research Foundation and the National Science Research Foundation (OTKA) of Hungary under grant Nos T-1999 and T-4420.

References

[1] Földvári I, Raksányi K, Voszka R, Hartmann E and Péter Á 1981 *J. Cryst. Growth* **52** 561
[2] Malicskó L and Krajewski Th 1982 *J. Cryst. Growth* **60** 195
[3] Földvári I, Voszka R and Péter Á 1982 *J. Cryst. Growth* **59** 651
[4] Földvári I, Cravero I, Watterich A and Morlin Z 1983 *Radiat. Eff.* **73** 161
[5] Watterich A, Voszka R, Söthe H and Spaeth J-M 1987 *J. Phys. C: Solid State Phys.* **20** 3155
[6] Edwards G J, Gilliam O R, Bartram R H, Watterich A, Voszka R, Niklas J R, Greulich-Weber S and Spaeth J-M 1995 *J. Phys.: Condens. Matter* **7** to appear
[7] Watterich A, Raksányi K, Gilliam O R, Bartram R H, Kappers L A, Söthe H and Spaeth J-M 1992 *J. Phys. Chem. Solids* **53** 189
[8] Lindquist O 1968 *Acta Chem. Scand.* **22** 977
[9] Carter D L and Okaya A 1960 *Phys. Rev.* **118** 1485
[10] Andersson P O and Kollberg E L 1973 *Phys. Rev.* B **8** 4956
[11] Rhein W and Rosinski Ch 1972 *Phys. Status Solidi* b **49** 667
[12] Rhein W Z 1972 Z. *Naturf.* a **27** 741
[13] Schmidt F and Voszka R 1981 *Cryst. Res. Technol.* **16** K127
[14] Altschuler S and Kozyrev B M 1974 *Electron Paramagnetic Resonance in Compounds of Transition Elements* (New York: Wiley) 1972 Russian orig. (Moscow: Nauka)
[15] Grachev V G 1987 *Zh. Eskp. Teor. Fiz.* **92** 1834; 1987 *Sov. Phys.–JETP* **65** 1029
[16] Murtagh B A and Sargent R W H 1970 *Comput. J.* **13** 185
[17] Lide D R (ed) 1994 *Handbook of Chemistry and Physics* 75th edn (Boca Raton, FL: Chemical Rubber Company)
[18] Andersson P O, Kollberg E L and Jelenski A 1974 *J. Phys. C: Solid State Phys.* **7** 1868
[19] Lippincott E R and Schroeder R 1955 *J. Chem. Phys.* **23** 1099
[20] Kirkpatrick E S, Müller K A and Rubins R S 1964 *Phys. Rev.* A **135** 86
[21] Hikita H, Takeda K and Kimura Y 1990 *Phys. Status Solidi* a **119** 251
[22] Watterich A, Bartram R H, Edwards G J, Gilliam O R, Földvári I and Voszka R 1987 *J. Phys. Chem. Solids* **48** 249